

Symmetry oscillations in strongly interacting one-dimensional mixtures

S. Musolino,^{1,2} M. Albert,^{2,3} A. Minguzzi,¹ and P. Vignolo^{2,3}

¹*Université Grenoble Alpes, CNRS, LPMMC, 38000 Grenoble, France*

²*Université Côte d'Azur, CNRS, Institut de Physique de Nice, 06200 Nice, France*

³*Institut Universitaire de France*

(Dated: July 2, 2024)

Multi-component quantum mixtures in one dimension can be characterized by their symmetry under particle exchange. For a strongly-interacting Bose-Bose mixture, we show that the time evolution of the momentum distribution from an initially symmetry-mixed state is quasi-constant for a $SU(2)$ symmetry conserving Hamiltonian, while it displays large oscillations in time for the symmetry-breaking case where inter- and intra-species interactions are different. Using the property that the momentum distribution operator at strong interactions commutes with the class-sum operator, the latter acting as a symmetry witness, we show that the momentum distribution oscillations correspond to symmetry oscillations, with a mechanism analog to neutrino flavour oscillations.

In quantum mechanics, when the initial state is not an eigenstate of the time-evolving operator, its time evolution displays oscillations, signalling quantum coherence of the state. From Rabi oscillations among single-particle states to Josephson oscillations in an emerging effective two-level system, such oscillations are used for a wealth of applications: from qubits [1] to metrology standards [2]. Quantum mechanical oscillations may occur as well among other degrees of freedom, for example, neutrino oscillations are due to the fact that the flavour basis in which neutrinos are defined does not coincide with the basis of their evolution [3]. In this Letter, we focus on symmetry oscillations, i.e. oscillations among states with a defined symmetry under particle exchange. Particle exchange symmetry is a crucial property of many-body systems: while the wavefunction of indistinguishable bosons (spin-polarized fermions) is totally symmetric (antisymmetric) under exchange, the one of multi-component mixtures has a symmetry under exchange among different types of particles that is not a priori specified [4].

Strongly interacting mixtures in one dimension (1D) represent a special class of systems where symmetry aspects can be unambiguously investigated. The versatility and controllability of ultracold atoms made it possible to reach the strongly interacting regime in experiments both for bosonic and fermionic particles [5–7], and several aspects have been studied ever-since, both at equilibrium [8–10] and out of equilibrium [11–13]. Theoretically, 1D systems may be described by a wealth of complementary methods, both analytical, as bosonization and exact solutions [14–17], and numerical [18, 19]. Strongly repulsive contact interactions give rise to a gas of impenetrable particles whose wave function vanishes when two particles approach each other. This corresponds to the celebrated Tonks-Girardeau (TG) [20, 21] regime, first discovered for single-component bosons and then extended to multi-component mixtures [22–24]. In the TG limit, the many-body wave function of a mixture factorizes in an orbital and spin part. The orbital part can be exactly written by mapping onto the one of non-interacting

fermions in the same external potential, while, for a two-component mixture, the spin part is described by the Hamiltonian of an effective spin chain, where site index corresponds to particle index and hopping coefficients are fixed by the gradients of the many-body wavefunction upon particle exchange [23, 24]. A similar mapping has also been extended to $SU(N)$ mixtures [25, 26]. Due to particle-exchange symmetry, a given many-body state of a mixture can be classified in terms of irreducible representations of the symmetry group of permutations of N elements, S_N , each associated to a different Young diagram [26–30]. Suitable symmetry witness operators are the class-sum operators [31], which probe particle permutation cycles. Whilst spin degrees of freedom do not affect the total density of the system, which coincides with the one of the mapped Fermi gas, the spatially non-local correlation functions, such as the one-body density matrix and, consequently, the momentum distribution of the interacting mixture differ considerably from those of a non-interacting Fermi gas.

In this Letter, we focus on the momentum distribution of a strongly interacting 1D Bose-Bose mixture, and show that it is an ideal observable to probe the symmetry of the state, since the momentum distribution operator and the symmetry witness can be simultaneously diagonalized. We monitor both its peak at zero momentum, which characterizes the presence of quasi off-diagonal long-range order, and its tails at large momenta, which show a universal power law decay and give information on short-range correlations. We propose a quench protocol in which, starting from an initial state with several symmetry components, we let the state evolve and follow the dynamics of the momentum distribution. We show that the time evolution is very different depending whether the system Hamiltonian is $SU(2)$ symmetric, i.e. with equal inter and intra-species interactions, or symmetry breaking, i.e. with different inter and intra-species interactions. The momentum distribution remains approximately constant in time for the $SU(2)$ case, while it oscillates for the symmetry-broken case. In both cases,

the dynamical evolution of the momentum distribution is very close to the one of the symmetry witness.

Model.— We consider a 1D mixture of N bosonic particles with two equally-balanced components (\uparrow and \downarrow) of mass m interacting via repulsive contact interactions as described by the Hamiltonian

$$H = \sum_{i=1}^N \left[-\frac{\hbar^2}{2m} \frac{\partial^2}{\partial x_i^2} + V(x_i, t) \right] + g_{\uparrow\downarrow} \sum_{i,j} \delta(x_{i,\uparrow} - x_{j,\downarrow}) + \sum_{\sigma=\uparrow,\downarrow} g_{\sigma\sigma} \sum_{i<j} \delta(x_{i,\sigma} - x_{j,\sigma}), \quad (1)$$

where $V(x_i, t)$ is a spin-independent external trapping potential, and $g_{\sigma\sigma'}$ is the inter- ($\sigma \neq \sigma'$) or intra-species ($\sigma = \sigma'$) interaction strength. In the limit of $g_{\sigma\sigma'} \rightarrow +\infty$, for any σ, σ' , the many-body wave-function Ψ vanishes whenever $x_i = x_j$. Using a generalized time-dependent Bose-Fermi mapping [23, 24, 32], the time-evolving exact many-body wavefunction can be written as

$$\Psi(\vec{X}, \vec{\sigma}, t) = \sum_{P \in S_N} \langle \vec{\sigma} | \hat{P} | \chi(t) \rangle \theta_P(\vec{X}) \Psi_A(\vec{X}, t), \quad (2)$$

which allows us to describe a system with spatial ($\vec{X} \equiv \{x_1, \dots, x_N\}$) and spin ($\vec{\sigma} \equiv \{\sigma_1, \dots, \sigma_N\}$) degrees of freedom. The operator \hat{P} in Eq. (2) corresponds to a permutation in S_N , $|\chi(t)\rangle$ is the spin state at time t , $\theta_P(\vec{X})$ is the generalized Heaviside function, which is equal to 1 in the coordinate sector $x_{P(1)} < \dots < x_{P(N)}$ and 0 elsewhere, and $\Psi_A = A\Psi_F$ with $A = \prod_{i<j} \text{sgn}(x_i - x_j)$. Finally, $\Psi_F = (1/\sqrt{N!}) \det[\phi_j(x_k, t)]$ is the wave-function of N spinless noninteracting fermions, built from the single particle orbitals $\phi_j(x, t)$ for a quantum particle in the potential $V(x, t)$, time evolved from an initial Fermi sphere configuration [32].

In the limit of strongly repulsive interactions, Eq. (1) can be mapped to an effective spin Hamiltonian, in a Hilbert space of dimension $M = N!/(N_\uparrow!N_\downarrow!)$, where the site index corresponds to the particle index [30, 33–35], which for $g_{\uparrow\uparrow} = g_{\downarrow\downarrow} = g$ reads

$$H_s = - \sum_{i=1}^{N-1} 2\alpha_i \left[\frac{1}{g_{\uparrow\downarrow}} (S_i^x S_{i+1}^x + S_i^y S_{i+1}^y) + \left(\frac{2}{g} - \frac{1}{g_{\uparrow\downarrow}} \right) S_i^z S_{i+1}^z + \left(\frac{1}{4g_{\uparrow\downarrow}} + \frac{1}{2g} \right) \right], \quad (3)$$

where the couplings α_i are given by

$$\alpha_i = \frac{N!\hbar^4}{m^2} \int d\vec{X} \theta_{\text{id}}(\vec{X}) \delta(x_i - x_{i+1}) \left| \frac{\partial \Psi_A}{\partial x_i} \right|^2. \quad (4)$$

Notice that if $g = g_{\uparrow\downarrow}$ the effective spin Hamiltonian (3) is a $SU(2)$ -symmetric XXX Heisenberg chain H_{SU} , while in the general case $g \neq g_{\uparrow\downarrow}$ it corresponds to a XXZ

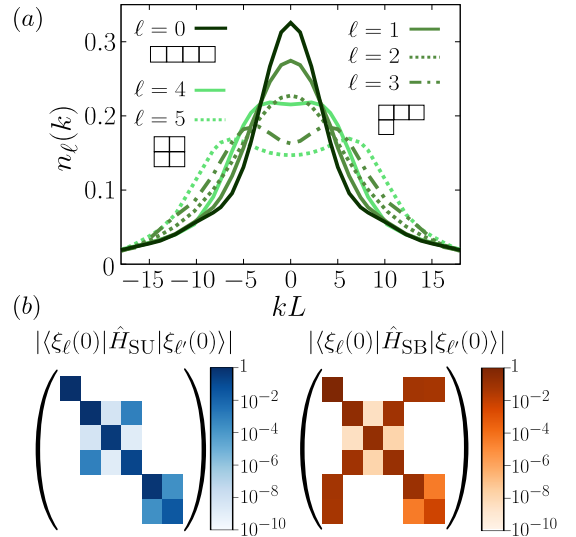


Figure 1. (a) Symmetry-resolved momentum distribution $n_\ell(k)$ (see Eq. (9)) for $N = 4$ bosons. The corresponding Young diagrams are also represented in the legend. (b) Absolute value of the matrix elements of the $SU(2)$ (left) and the symmetry-breaking (right) Hamiltonian (dimensionless, normalized to the value of the largest element) in the basis of $|\xi_\ell(k)\rangle$ at $k = 0$ in logarithmic scale. In both panels, the indices ℓ are sorted in a way that $\ell = 0$ corresponds to the $\Gamma^{(2)}$ -eigenvalue $\gamma_0 = 6$ (the most symmetric one), $\ell = 1, 2, 3$ to $\gamma_{1,2,3} = 2$, and $\ell = 4, 5$ to $\gamma_{4,5} = 0$ (the most antisymmetric).

chain H_{SB} , which breaks the $SU(2)$ symmetry. The time evolution of the spin part of the many-body wavefunction is given by $|\chi(t)\rangle = e^{-i\hat{H}_s t} |\chi(0)\rangle$, where $|\chi(0)\rangle$ is the spin configuration of the initial state.

Observables and symmetry witness.— We demonstrate here that the total momentum distribution, given by the Fourier transform of the one-body density matrix $\rho^{(1)}(x, x', t) = \langle \Psi | \sum_\sigma \sum_{i=1}^N (|x, \sigma\rangle \langle x', \sigma|)_i | \Psi \rangle$ in the case of a strongly interacting mixture gives direct access to the symmetry content of the state. Indeed, using Eq. (2), the total momentum distribution reads $n(k, t) = \langle \chi(t) | \hat{n}_k | \chi(t) \rangle$, where the momentum density operator in spin space is given by [36]

$$\hat{n}_k = \sum_{i,j=1}^N \hat{P}_{(i,\dots,j)} R^{(i,j)}(k), \quad (5)$$

where $\hat{P}_{(i,\dots,j)}$ is the cyclic (anticyclic) permutation $i \rightarrow i+1 \rightarrow \dots \rightarrow j-1 \rightarrow j \rightarrow i$ ($i \rightarrow i-1 \rightarrow \dots \rightarrow j+1 \rightarrow j \rightarrow i$) if $i < j$ ($i > j$) and the identity if $i = j$. The orbital part is given by

$$R^{(i,j)}(k) = \frac{N!}{2\pi} \int dx dx' e^{-ik(x-x')} \int_{I_{ij}} \left(\prod_{n \neq i} dx_n \right) \Psi_A(x_1, \dots, x_{i-1}, x, x_{i+1}, \dots, x_N) \times \Psi_A(x_1, \dots, x_{i-1}, x', x_{i+1}, \dots, x_N), \quad (6)$$

with I_{ij} is the integration interval defined by $x_1 < \dots < x_{i-1} < x < x_{i+1} < \dots < x_{j-1} < x' < x_j < \dots < x_N$ ($i < j$) [36]. Notice that $R^{(i,j)}(k)$ fixes the type of permutation cycles contributing to the momentum distribution at a given k . At large k , only binary permutations $i \rightarrow i+1$ have non-zero weight: the only particle exchanges that matter at short distances are those involving two particles, which are responsible for building the large-momentum tails $n(k) = Ck^{-4}$ where $C = C_T + C_b$ is given by the two-body Tan contact C_T and, in a box trap, additional boundary terms C_b [37, 38]. At $k=0$, instead, all permutation cycles play a role: in order to establish quasi-off-diagonal long-range order one needs to sample the coherence established among all the particles [30]. We also recall that $R^{(i,j)}(k)$ may be time-dependent if the dynamical evolution involves variations of the external trapping potential.

In order to characterize the symmetry of the mixture, we use a set of generators of the $SU(2)$ algebra related to the permutation symmetry group. In particular, we take as symmetry witness the two-cycle class sum operator, which corresponds to the group partition related to the sum of the transpositions $\hat{P}_{i,j}$ [26, 28, 30], namely

$$\hat{\Gamma}^{(2)} = \sum_{i < j} \hat{P}_{i,j}. \quad (7)$$

The crucial observation for the following derivation is that the momentum density operator \hat{n}_k has the property [39]

$$[\hat{\Gamma}^{(2)}, \hat{n}_k] = 0. \quad (8)$$

Therefore, one can make the following symmetry decomposition of the momentum distribution:

$$n(k, t) = \sum_{\ell=1}^M |\langle \chi(t) | \xi_{\ell}(k) \rangle|^2 n_{\ell}(k), \quad (9)$$

where the basis $\{|\xi_{\ell}(k)\rangle\}$ diagonalizes both \hat{n}_k and $\hat{\Gamma}^{(2)}$, such that $\hat{n}_k |\xi_{\ell}(k)\rangle = n_{\ell}(k) |\xi_{\ell}(k)\rangle$ and $\hat{\Gamma}^{(2)} |\xi_{\ell}(k)\rangle = \gamma_{\ell} |\xi_{\ell}(k)\rangle$. Figure 1(a) shows the symmetry-resolved momentum distributions $n_{\ell}(k)$ for a bosonic mixture with $N_{\uparrow} = 2$ and $N_{\downarrow} = 2$. Interestingly, the most symmetric configuration has a single peak at $k=0$, while the most antisymmetric one – compatible with bosonic exchange symmetry – has as many peaks as the number of particles in each component, as it has been previously noted for fermionic mixtures [36, 40]. In the time evolution under a symmetry-breaking Hamiltonian, the quantum state explores different symmetry components and the momentum distribution oscillates among the various shapes shown in Fig. 1(a).

The result (8) is non-trivial. Notice, for example, that the $SU(2)$ Hamiltonian, also constructed with permutation operators as the symmetry witness, does not commute with \hat{n}_k , and, therefore, one cannot find a

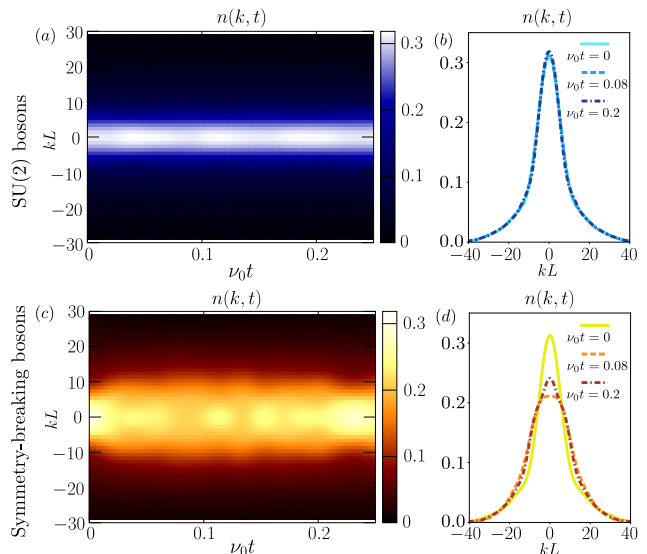


Figure 2. Time evolution of the momentum distribution $n(k, t)$ for 3 + 3 $SU(2)$ bosons [(a) and (b)] and symmetry breaking bosons [(c) and (d)] trapped in a box with size L for an initial state $|\chi(0)\rangle = |\uparrow\uparrow\downarrow\downarrow\rangle$. (a)-(c) Momentum-time map of $n(k, t)$. (b)-(d) $n(k, t)$ at given time in the dynamics as indicated in the legend of the figures (b) and (d). The time is in units of $\nu_0 = \hbar/(mL^2)$.

basis that simultaneously diagonalizes \hat{H}_{SU} , $\hat{\Gamma}^{(2)}$ and \hat{n}_k [39]. Figure 1(b) shows the matrix elements $\epsilon^{\ell, \ell'}(k) = |\langle \xi_{\ell}(k) | \hat{H} | \xi_{\ell'}(k) \rangle|$ for $k=0$ and $N=4$ of both the $SU(2)$ Hamiltonian and the SB Hamiltonian. We notice that, for \hat{H}_{SU} , the nonzero off-diagonal terms are smaller with respect to the diagonal terms and are nonzero only inside the same symmetry sector, following from the fact that $[\hat{H}_{SU}, \hat{\Gamma}^{(2)}] = 0$. Contrarily, for \hat{H}_{SB} , not only the off-diagonal terms are comparable in magnitude to the diagonal terms, but there is also coupling between different symmetries. As a consequence, the dynamics of the momentum distribution predicted in Eq.(9) will be very different in the $SU(2)$ -symmetric and symmetry broken case.

Momentum distribution dynamics and symmetry oscillations. – In order to observe symmetry oscillations, we solve exactly the dynamics of a strongly interacting Bose-Bose mixture in a box trap, prepared initially in a symmetry-mixed configuration, and evolving either under the $SU(2)$ Hamiltonian, i.e. where we take $g = g_{\uparrow\downarrow}$ or the SB Hamiltonian, where we take $g \rightarrow \infty$ and $g_{\uparrow\downarrow}$ large but finite, as in Ref. [30]. We choose as initial state the configuration with all spin-up particles on the left and spin-down on the right, namely $|\chi(0)\rangle = |\uparrow\uparrow\downarrow\downarrow\rangle$, which is of experimental relevance [41]. Since there is no change in the external potential, the dynamics occurs only among spin components, the only time-dependent part of Eq. (2) are the spin coefficients, $\langle \vec{\sigma} | \hat{P} | \chi(t) \rangle$. In real space, the dynamics gives rise to spin mixing and oscillations of the magnetization, analogous to what was

observed in Ref. [42] for fermionic mixtures.

The dynamics in momentum space is illustrated in Fig. 2, where we show the evolution in momentum-time maps and at selected times. While in the case of the $SU(2)$ -symmetric mixture the dynamics is practically constant (see below for more details), clear oscillations are seen in the momentum distribution of the symmetry-broken case. Such oscillations are particularly visible at small momenta, but actually affect the whole momentum distribution down to its tails.

To infer the relation of such oscillations with the symmetry oscillations, we follow comparatively in Fig. 3 the time evolution of the expectation value of the symmetry witness

$$\gamma^{(2)}(t) = \langle \chi(t) | \hat{\Gamma}^{(2)} | \chi(t) \rangle, \quad (10)$$

together with the value of the momentum distribution at $k = 0$ and of the weight of the large-momentum tails $\mathcal{C}(t) = \lim_{k \rightarrow \infty} k^4 n(k, t)$. For the reference case of a $SU(2)$ -symmetric Hamiltonian, the symmetry witness is constant in time since $[\hat{H}_{SU}, \hat{\Gamma}^{(2)}] = 0$. Also the Tan contact is constant in time, as readily follows from the fact that the only non-zero term of Eq. (5) at large momenta is $R^{(i, i+1)}(k)$, which implies that the Tan contact is proportional to the $SU(2)$ Hamiltonian, as readily follows by recalling that the latter can be rewritten – taken apart a constant term which is irrelevant in our discussion – as $H_{SU} = \sum_i J_i P_{i, i+1}$, with $J_i = \alpha_i/g$. The peak of the momentum distribution instead displays small oscillations. These are due to the fact that $[\hat{H}_{SU}, \hat{n}_k] \neq 0$, and correspond to oscillations *within* a symmetry sector of the Hamiltonian represented in Fig. 1.

The dynamics of the symmetry-broken case shows a striking similarity among the time evolution of $\gamma^{(2)}(t)$, $\mathcal{C}(t)$ and $n(k = 0, t)$. The minor differences among them is due to the fact that the symmetry weights in $\gamma^{(2)}(t) = \sum_{\ell=1}^M |\langle \chi(t) | \xi_{\ell}(k) \rangle|^2 \gamma_{\ell}$ and in $n(k, t) = \sum_{\ell=1}^M |\langle \chi(t) | \xi_{\ell}(k) \rangle|^2 n_{\ell}(k)$ are different and in particular, the γ_{ℓ} may have degenerate values. The close similarity of the three curves confirms that the momentum distribution oscillations correspond to particle-exchange symmetry oscillations.

Conclusions. – In this work we have demonstrated that the dynamics of the total momentum distribution of a strongly interacting mixture with broken $SU(2)$ symmetry can be used to probe particle-exchange symmetry oscillations, induced by the time evolution of an initially symmetry-mixed state. We have shown that the oscillations are visible both in the zero-momentum peak and in the tails of the momentum distribution, and faithfully reflect the oscillations of the symmetry witness operator $\hat{\Gamma}^{(2)}$. Our predictions are relevant for experiments with multi-component ultracold atoms [43, 44], where the interatomic interactions can be tuned using Feshbach resonances and the time evolution of the momentum distribution is accessible using time-of-flight experiments. Our

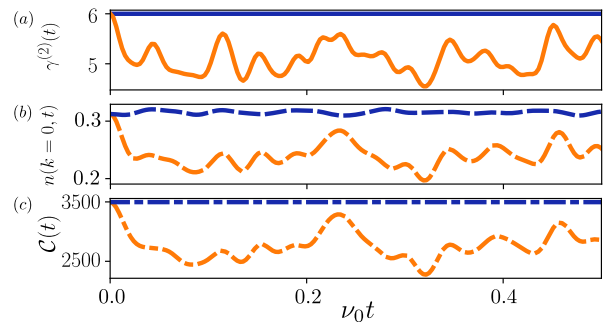


Figure 3. Time evolution of the (a) expectation value of $\hat{\Gamma}^{(2)}$ on the out-of-equilibrium state (Eq. (7), solid lines), (b) momentum distribution at $k = 0$ (dashed lines), and (c) weight of the large-momentum tails (dot-dashed lines). In all panels, the curves for $SU(2)$ bosons are in blue (upper curves) and for symmetry-breaking bosons in orange (lower curves).

result paves the way to the investigation of the interplay of symmetry and interactions in multi-component quantum systems.

We thank G. Aupetit-Diallo, J. Beugnon, F. Cataliotti, and J. Dalibard for valuable discussions. We acknowledge financial support from the ANR-21-CE47-0009 Quantum-SOPHA project and the support of the Institut Henri Poincaré (UAR 839 CNRS-Sorbonne Université), and LabEx CARMIN (ANR-10-LABX-59-01).

-
- [1] M. H. Devoret and J. M. Martinis, *Quantum Information Processing* **3**, 163 (2004).
 - [2] L. Pezzè, A. Smerzi, M. K. Oberthaler, R. Schmied, and P. Treutlein, *Rev. Mod. Phys.* **90**, 035005 (2018).
 - [3] P. D. Group, R. L. Workman, V. D. Burkert, V. Crede, E. Klempt, U. Thoma, L. Tiator, K. Agashe, G. Aielli, and B. Allanach et al., *Progress of Theoretical and Experimental Physics* **2022**, 083C01 (2022).
 - [4] B. Sutherland, *Phys. Rev. Lett.* **20**, 98 (1968).
 - [5] T. Kinoshita, T. Wenger, and D. Weiss, *Science* **305**, 1125 (2004).
 - [6] B. Paredes, A. Widera, V. Murg, O. Mandel, S. Fölling, I. Cirac, G. V. Shlyapnikov, T. Hansch, and I. Bloch, *Nature* **429**, 277 (2004).
 - [7] G. Zürn, F. Serwane, T. Lompe, A. N. Wenz, M. G. Ries, J. E. Bohn, and S. Jochim, *Phys. Rev. Lett.* **108**, 075303 (2012).
 - [8] T. Kinoshita, T. Wenger, and D. S. Weiss, *Phys. Rev. Lett.* **95**, 190406 (2005).
 - [9] E. Haller, M. Gustavsson, M. J. Mark, J. G. Danzl, R. Hart, G. Pupillo, and H.-C. Nägerl, *Science* **325**, 1224–1227 (2009).
 - [10] T. Jacqmin, J. Armijo, T. Berrada, K. V. Kheruntsyan, and I. Bouchoule, *Phys. Rev. Lett.* **106**, 230405 (2011).
 - [11] T. Kinoshita, T. Wenger, and D. S. Weiss, *Nature* **440**, 900 (2006).
 - [12] J. M. Wilson, N. Malvania, Y. Le, Y. Zhang, M. Rigol, and D. S. Weiss, *Science* **367**, 1461–1464 (2020).
 - [13] I. Bouchoule and J. Dubail, *Journal of Statistical Me-*

- chanics: Theory and Experiment **2022**, 014003 (2022).
- [14] T. Giamarchi, *Quantum Physics in One Dimension* (Oxford University Press, 2003).
- [15] T. Sowiński and M. Ángel García-March, Reports on Progress in Physics **82**, 104401 (2019).
- [16] A. Minguzzi and P. Vignolo, AVS Quantum Science **4**, 027102 (2022).
- [17] S. Mistakidis, A. Volosniev, R. Barfknecht, T. Fogarty, T. Busch, A. Foerster, P. Schmelcher, and N. Zinner, Physics Reports **1042**, 1 (2023).
- [18] U. Schollwöck, Rev. Mod. Phys. **77**, 259 (2005).
- [19] J. I. Cirac, D. Pérez-García, N. Schuch, and F. Verstraete, Rev. Mod. Phys. **93**, 045003 (2021).
- [20] L. Tonks, Phys. Rev. **50**, 955 (1936).
- [21] M. Girardeau, Journal of Mathematical Physics **1**, 516 (1960).
- [22] M. D. Girardeau and A. Minguzzi, Phys. Rev. Lett. **99**, 230402 (2007).
- [23] F. Deuretzbacher, K. Fredenhagen, D. Becker, K. Bongs, K. Sengstock, and D. Pfannkuche, Phys. Rev. Lett. **100**, 160405 (2008).
- [24] A. G. Volosniev, D. V. Fedorov, A. S. Jensen, M. Valiente, and N. T. Zinner, Nat. Commun. **5** (2014), 10.1038/ncomms6300.
- [25] J. Decamp, P. Armagnat, B. Fang, M. Albert, A. Minguzzi, and P. Vignolo, New Journal of Physics **18**, 055011 (2016).
- [26] J. Decamp, J. Jünemann, M. Albert, M. Rizzi, A. Minguzzi, and P. Vignolo, Phys. Rev. A **94**, 053614 (2016).
- [27] M. Hamermesh, *Group Theory and Its Application to Physical Problems*, Addison Wesley Series in Physics (Dover Publications, 1989).
- [28] B. Fang, P. Vignolo, M. Gattobigio, C. Miniatura, and A. Minguzzi, Phys. Rev. A **84**, 023626 (2011).
- [29] N. L. Harshman, Few-Body Systems **57**, 11 (2015).
- [30] G. Aupetit-Diallo, G. Pecci, C. Pignol, F. Hébert, A. Minguzzi, M. Albert, and P. Vignolo, Phys. Rev. A **106**, 033312 (2022).
- [31] J. Katriel, Journal of Physics A: Mathematical and General **26**, L135 (1993).
- [32] M. D. Girardeau and E. M. Wright, Phys. Rev. Lett. **84**, 5239 (2000).
- [33] P. Massignan, J. Levinsen, and M. M. Parish, Phys. Rev. Lett. **115**, 247202 (2015).
- [34] L. Yang and X. Cui, Phys. Rev. A **93**, 013617 (2016).
- [35] R. E. Barfknecht, A. Foerster, and N. T. Zinner, Few-Body Systems **59** (2018), 10.1007/s00601-018-1352-4.
- [36] F. Deuretzbacher, D. Becker, and L. Santos, Phys. Rev. A **94**, 023606 (2016).
- [37] B. De Bruyne, D. S. Dean, P. Le Doussal, S. N. Majumdar, and G. Schehr, Phys. Rev. A **104**, 013314 (2021).
- [38] G. Aupetit-Diallo, S. Musolino, M. Albert, and P. Vignolo, Phys. Rev. A **107**, L061301 (2023).
- [39] See Supplemental Material at <http://link.aps.org/supplemental>, which includes Refs. [..], for additional information about the derivation of the equations.
- [40] J. Decamp, J. Jünemann, M. Albert, M. Rizzi, A. Minguzzi, and P. Vignolo, New Journal of Physics **19**, 125001 (2017).
- [41] A. Sommer, M. Ku, G. Roati, and M. W. Zwierlein, Nature **472**, 201–204 (2011).
- [42] G. Pecci, P. Vignolo, and A. Minguzzi, Phys. Rev. A **105**, L051303 (2022).
- [43] S. De, D. L. Campbell, R. M. Price, A. Putra, B. M. Anderson, and I. B. Spielman, Phys. Rev. A **89**, 033631 (2014).
- [44] R. Cominotti, C. Rogora, A. Zenesini, G. Lamporesi, and G. Ferrari, Europhysics Letters **146**, 45001 (2024).

Supplementary Material: “Symmetry oscillations in strongly interacting one-dimensional mixtures”

S. Musolino,^{1,2} M. Albert,^{2,3} A. Minguzzi,¹ and P. Vignolo^{2,3}

¹Université Grenoble Alpes, CNRS, LPMMC, 38000 Grenoble, France

²Université Côte d’Azur, CNRS, Institut de Physique de Nice, 06200 Nice, France

³Institut Universitaire de France

(Dated: July 2, 2024)

CONTENTS

I. Symmetry decomposition of the momentum distribution	1
A. Commutator with $\Gamma^{(2)}$	2
B. Commutator with \hat{H}_{SU}	3
II. Tan’s relation in the spin dynamics	5
III. Analytical expressions for $N = 4$	7
References	9

I. SYMMETRY DECOMPOSITION OF THE MOMENTUM DISTRIBUTION

In this Section, we show that the momentum distribution operator, \hat{n}_k (Eq. (5) of the main text), commutes with the two-cycle class-sum operator, $\hat{\Gamma}^{(2)}$ (Eq. (7) of the main text), but not with the SU(2) Hamiltonian, \hat{H}_{SU} .

First, we recall the definition of \hat{n}_k , namely

$$\hat{n}_k \equiv \sum_{i=1}^N \sum_{j=1}^N \hat{P}_{(i,\dots,j)} R^{(i,j)}(k), \quad (\text{S1})$$

where $P_{(i,\dots,j)}$ is the loop permutation defined as [1]

$$P_{(i,\dots,j)} = \begin{cases} P_{(i,i+1,\dots,j-1,j)} & \text{if } i < j \\ \text{id} & \text{if } i = j \\ P_{(i,i-1,\dots,j+1,j)} & \text{if } i > j \end{cases}, \quad (\text{S2})$$

which is a cyclic (anti-cyclic) permutation if $i < j$ ($i > j$), and $R^{(i,j)}(k)$ is the spatial part defined in Eq.(6) of the main text. For convenience, we re-write the sums over the loop permutations in Eq. (S1) as

$$\sum_{i=1}^N \sum_{j=1}^N P_{(i,\dots,j)} = N \times \text{id} + \sum_{m=1}^{N-1} \sum_{i=1}^{N-m} (P_{(i,i+1,\dots,i+m)} + P_{(i+m,i+m-1,\dots,i)}), \quad (\text{S3})$$

where we have distinguished the diagonal part with $m = 0$ ($i = j$), the cycle $i \rightarrow i+m$ ($i < j$) and its inverse $i+m \rightarrow i$ ($i > j$). From Eq. (S3), we now define a reduced form of the class-sum operators given by

$$\hat{\Gamma}_{\text{red}}^{(m+1)}(k) = \sum_{i=1}^{N-m} (\hat{P}_{(i,i+1,\dots,i+m)} + \hat{P}_{(i+m,i+m-1,\dots,i)}) R^{(i,i+m)}(k), \quad (\text{S4})$$

where $R^{(i,i+m)}(k) = R^{(i+m,i)}(k)$ due to parity. The momentum operator is therefore defined as $\hat{n}_k = N \hat{\Gamma}_{\text{red}}^{(i,i)}(k) + \sum_{m=1}^{N-1} \hat{\Gamma}_{\text{red}}^{(m+1)}$. We notice that the $\hat{\Gamma}_{\text{red}}^{(m+1)}(k)$ operators count only the cycles of degree m with ordered indices $i \rightarrow i+1 \rightarrow \dots \rightarrow i+m$, which are therefore less than the permutations counted by the corresponding class-sum operator.

We now show that for every m and k the operator in Eq. (S4) commutes with $\hat{\Gamma}^{(2)}$, namely

$$[\hat{\Gamma}^{(2)}, \hat{\Gamma}_{\text{red}}^{(m+1)}(k)] = 0, \quad (\text{S5})$$

and, consequently, $[\hat{\Gamma}^{(2)}, \hat{n}_k] = 0$, but does not commute with the SU(2)-symmetric Hamiltonian, namely

$$[\hat{H}_{\text{SU}}, \hat{\Gamma}_{\text{red}}^{(m+1)}(k)] \neq 0. \quad (\text{S6})$$

To calculate the commutators in Eqs. (S5) and (S6), we introduce the swap operators [2–4]

$$F_{\mu}^{\nu}(i) = \hat{a}_{i,\mu}^{\dagger} \hat{a}_{i,\nu}, \quad (\text{S7})$$

where $\hat{a}_{i,\nu}$ annihilates a boson with flavour ν at lattice site i . The operators $F_{\mu}^{\nu}(i)$ follows the commutation relation

$$[F_{\mu}^{\nu}(i), F_{\alpha}^{\beta}(j)] = \delta_{i,j} (F_{\mu}^{\beta}(i) \delta_{\alpha\nu} - F_{\alpha}^{\nu}(i) \delta_{\mu\beta}). \quad (\text{S8})$$

In this notation, the SU(2) Hamiltonian can be written as

$$\hat{H}_{\text{SU}} = \sum_{i=1}^{N-1} \sum_{\mu,\nu} F_{\mu}^{\nu}(i) F_{\nu}^{\mu}(i+1) \quad (\text{S9})$$

in units of the nearest-neighbours coupling J and where we have neglected the constant term. We extend the same notation to represent a cycle permutation as

$$P_{(i,i+1,\dots,i+m-1,i+m)} = \sum_{\alpha_0, \alpha_1, \dots, \alpha_m} F_{\alpha_0}^{\alpha_1}(i) F_{\alpha_1}^{\alpha_2}(i+1) \cdots F_{\alpha_{m-1}}^{\alpha_m}(i+m-1) F_{\alpha_m}^{\alpha_0}(i+m). \quad (\text{S10})$$

A. Commutator with $\Gamma^{(2)}$

Using Eq. (S10) and considering only the loop from $i \rightarrow i+m$ (the inverse loop can be calculated using analogous steps), we start the proof of Eq. (S5) by writing

$$\begin{aligned} [\hat{\Gamma}^{(2)}, \hat{\Gamma}_{\text{red}}^{(m+1)}(k)] &= \sum_{x=1}^{N-1} \sum_{y=2}^N \sum_{i=1}^{N-m} \sum_{\text{flav.}} \left([F_{\mu}^{\nu}(x) F_{\nu}^{\mu}(y), F_{\lambda}^{\alpha_1}(i) F_{\alpha_1}^{\alpha_2}(i+1) \cdots F_{\alpha_m}^{\lambda}(i+m)] \right) R^{(i,i+m)}(k) \\ &= \sum_{x=1}^{N-1} \sum_{y=2}^N \sum_{i=1}^{N-m} \sum_{\text{flav.}} \sum_{l=0}^m \left\{ \left(\prod_{s=0}^{l-1} F_{g(s)[1]}^{g(s)[2]}(i+s) \right) [F_{\mu}^{\nu}(x) F_{\nu}^{\mu}(y), F_{\alpha_l}^{\alpha_{l+1}}(i+l)] \right. \\ &\quad \left. \times \left(\prod_{t=l+1}^m F_{h(t)[1]}^{h(t)[2]}(i+t) \right) \right\} R^{(i,i+m)}(k), \end{aligned} \quad (\text{S11})$$

where we have used the linearity of the commutator and where $g(s) = \{(\lambda, \alpha_1), (\alpha_1, \alpha_2), \dots, (\alpha_{l-1}, \alpha_l)\}$ and $h(t) = \{(\alpha_{l+1}, \alpha_{l+2}), (\alpha_{l+2}, \alpha_{l+3}), \dots, (\alpha_m, \lambda)\}$ are bi-dimensional arrays containing the two pairs of indices for every s or t , and the sum over “flav.” means that all flavours (labelled by the Greek letters) are summed. We now can expand the commutator in the middle of Eq. (S11) for the l -th index in the following 4 terms

$$[F_{\mu}^{\nu}(x) F_{\nu}^{\mu}(y), F_{\alpha_l}^{\alpha_{l+1}}(i+l)] = \underbrace{F_{\alpha_l}^{\nu}(x) F_{\nu}^{\alpha_{l+1}}(i+l)}_{(a)} - \underbrace{F_{\alpha_l}^{\nu}(i+l) F_{\nu}^{\alpha_{l+1}}(x)}_{(b)} + \underbrace{F_{\alpha_l}^{\nu}(y) F_{\nu}^{\alpha_{l+1}}(i+l)}_{(c)} - \underbrace{F_{\alpha_l}^{\nu}(i+l) F_{\nu}^{\alpha_{l+1}}(y)}_{(d)}, \quad (\text{S12})$$

where the (c) and (d) terms are identical to (a) and (b) after the change of variable $y \rightarrow x$. The (a) and (b) terms are schematically represented in Fig. S1. For the cycle, the l -th (a) term is equal in modulus and opposite in sign to the $(l-1)$ -th (b) term and the same happens for the l -th (b) term and the $(l+1)$ -th (a) terms. Therefore, they all cancel each other out in neighboring pairs except for the (a) term with $l=0$ and the (b) term with $l=m$, which they cancel each other out due to the property of the cycle, indeed they correspond to the same cycle, namely $P_{(x,i,i+1,\dots,i+m)} = P_{(i,i+1,\dots,i+m,x)}$.

We can repeat the same procedure for the terms dependent on y and the inverse cycles. Therefore, the commutator in Eq. (S5) goes to zero for every m and without adding any constraints on the orbital part $R^{(i,i+m)}(k)$.



Figure S1: Schematic representation of the (a) and (b) cycles presented in the commutator $[\hat{\Gamma}^{(2)}, \hat{\Gamma}_{\text{red}}^{(m+1)}]$ (Eq. (S11)), and labelled according to the terms of Eq. (S12). Every arrow represents a transposition that connects two neighboring sites, represented by the rectangles. The (c) and (d) terms of Eq. (S12) are equivalent to (a) and (b) after the variable change $x \rightarrow y$.

B. Commutator with \hat{H}_{SU}

We now focus on Eq. (S6), where \hat{H}_{SU} is defined in Eq. (S9). We notice that the case $m = 1$ is trivial and corresponds to the commutator of the Hamiltonian with itself. In order to compute the commutator, we follow the same procedure used above and we write

$$\begin{aligned}
[\hat{H}_{\text{SU}}, \hat{\Gamma}_{\text{red}}^{(m+1)}(k)] &= \sum_{x=1}^{N-1} \sum_{i=1}^{N-m} \sum_{\text{flav.}} \left([F_{\mu}^{\nu}(x)F_{\nu}^{\mu}(x+1), F_{\lambda}^{\alpha_1}(i)F_{\alpha_1}^{\alpha_2}(i+1) \cdots F_{\alpha_m}^{\lambda}(i+m)] \right) R^{(i,i+m)}(k) \\
&= \sum_{l=1}^{N-1} \sum_{i=1}^{N-m} \sum_{\text{flav.}} \sum_{l=0}^m \left\{ \left(\prod_{s=0}^{l-1} F_{g(s)[1]}^{g(s)[2]}(i+s) \right) [F_{\mu}^{\nu}(x)F_{\nu}^{\mu}(x+1), F_{\alpha_l}^{\alpha_{l+1}}(i+l)] \right\} \\
&\times \left(\prod_{t=l+1}^m F_{h(t)[1]}^{h(t)[2]}(i+t) \right) \left\} R^{(i,i+m)}(k),
\end{aligned} \tag{S13}$$

where the Greek indices are defined as in Eq. (S11) and the l -th commutator in the middle gives

$$\begin{aligned}
[F_{\mu}^{\nu}(x)F_{\nu}^{\mu}(x+1), F_{\alpha_l}^{\alpha_{l+1}}(i+l)] &= \underbrace{\left(F_{\alpha_l}^{\nu}(i+l-1)F_{\nu}^{\alpha_{l+1}}(i+l) \right)}_{(a)} - \underbrace{\left(F_{\alpha_l}^{\nu}(i+l)F_{\nu}^{\alpha_{l+1}}(i+l-1) \right)}_{(b)} \\
&+ \underbrace{\left(F_{\alpha_l}^{\nu}(i+l+1)F_{\nu}^{\alpha_{l+1}}(i+l) \right)}_{(c)} - \underbrace{\left(F_{\alpha_l}^{\nu}(i+l)F_{\nu}^{\alpha_{l+1}}(i+l+1) \right)}_{(d)},
\end{aligned} \tag{S14}$$

whose terms are represented in Fig. S2. It is evident from the picture that the cycles are more complicated than the ones in Fig. S1. We first consider the middle terms of the sum over l , namely $l = 1, \dots, m-1$ and show that the (a)-(b) terms go to zero at given l . We will consider the remaining terms, which we call *border terms*, at the end of the section.

We notice that the l -th (a) and (d) terms contain an identity operator $P_{i+l-1, i+l-1} = \text{id}$ represented by the rounded link between the same node in Fig. S2. This can be also understood by considering that the operators in Eq. (S7) are constrained by $\sum_{\mu} \hat{a}_{i,\mu}^{\dagger} \hat{a}_{i,\mu} = 1$ [4], which yield to

$$\sum_{\alpha} F_{\gamma}^{\alpha}(i+l)F_{\alpha}^{\nu}(i+l) = 2F_{\gamma}^{\nu}(i+l). \tag{S15}$$

Therefore, the sum (a)+(d) is equal to zero for every l . Notice that so far we did not need to make any assumption on the spatial weight $R^{(i,i+m)}(k)$.

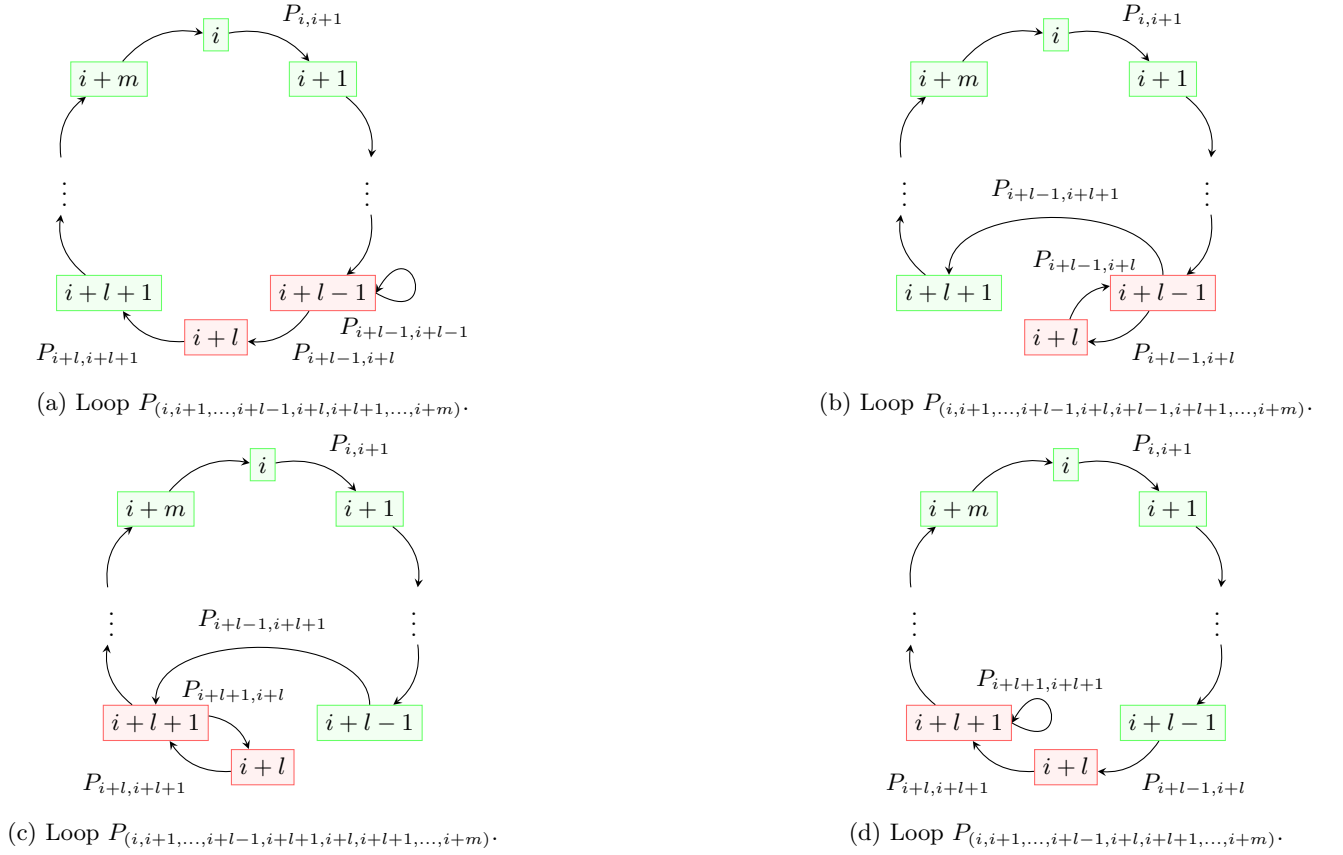


Figure S2: Schematic representation of the (a)-(d) cycles presented in the commutator $[\hat{H}_{\text{SU}}, \hat{\Gamma}_{\text{red}}^{(m+1)}]$ (Eq. (S13)), and labelled according to the four terms of Eq. (S14). Every arrow represents a transposition that connects two neighboring sites, represented by the rectangles.

The (b) and (c) terms also contain an identity operator, indeed

$$\begin{aligned} (b) \quad P_{(i,i+1,\dots,i+l-1,i+l,i+l-1,i+l+1,\dots,i+m)} &= \cdots P_{i+l-2,i+l-1} (P_{i+l-1,i+l} P_{i+l,i+l-1}) P_{i+l-1,i+l-1} \cdots \\ &= P_{(i,i+1,\dots,i+l-1,i+l+1,\dots,i+m)}, \end{aligned} \quad (\text{S16})$$

and

$$\begin{aligned} (c) \quad P_{(i,i+1,\dots,i+l-1,i+l+1,i+l,i+l+1,\dots,i+m)} &= \cdots P_{i+l-2,i+l-1} (P_{i+l-1,i+l+1} P_{i+l+1,i+l}) P_{i+l,i+l+1} \cdots \\ &= P_{(i,i+1,\dots,i+l-1,i+l+1,\dots,i+m)}, \end{aligned} \quad (\text{S17})$$

where we have used for the terms in parenthesis that $P_{i+l-1,i+l} P_{i+l,i+l-1} = P_{i+l-1,i+l} P_{i+l-1,i+l}^{-1} = \text{id}$ and, consequently, the two are the same cycle. Therefore, (b) and (c) terms for $0 < l < m$ are equal in modulus and opposite in sign. The same steps can be repeated for the intermediate terms of the inverse cycle.

Finally, we consider the border terms, namely the terms with $l = 0$ and $l = m$. From Eq. (S14), we find that

- the (a) term with $l = 0$ and the (d) term with $l = m$ contain the same cycle if we switch $j \rightarrow i + 1$ and this will give a term

$$\sum_{i=1}^{N-m-1} P_{i \rightarrow i+m+1} (R^{(i+1,i+1+m)}(k) - R^{(i,i+m)}(k)), \quad (\text{S18})$$

which is nonzero for different $R^{(i,j)}(k)$.

- The (a) term with $l = m$ and the (d) term with $l = 0$ cancel one another out after using Eq. (S15) for the indices $i + 1$ and $i + m - 1$, respectively.

- The (c) term with $l = 0$ is related to the cycle $P_{i+1,i}P_{i,i+1}P_{i+1,i+2}\dots P_{i+m-1,i+m} = P_{i+1\rightarrow i+m}$ where we have used $P_{i+1,i}P_{i,i+1} = \text{id}$ and the (b) term with $l = m$ contains a similar structured cycle $P_{i,i+1}P_{i+1,i+2}\dots P_{i+m-1,i+m}P_{i+m,i+m-1} = P_{i\rightarrow i+m-1}$ where we have used $P_{i+m,i+m-1}P_{i+m-1,i+m} = \text{id}$. Therefore, if we switch $j \rightarrow i - 1$ we can write them in terms of the same cycle $P_{i+1\rightarrow i+m}$. By also taking into account additional terms from the extremes of the sum, we obtain the contribution

$$\sum_{i=1}^{N-m-1} P_{i+1\rightarrow i+m}(R^{(i,i+m)}(k) - R^{(i+1,i+m+1)}(k)) + P_{N-m+1\rightarrow N}R^{(N-m,N)}(k) - P_{1\rightarrow m}R^{(1,1+m)}(k), \quad (\text{S19})$$

which is also nonzero in general.

- Finally, the remaining terms: (b) with $l = 0$ and (c) with $l = m$ give another nonzero contribution, namely

$$\sum_{i=1}^{N-m} (P_{(i,i+1,\dots,i+m-1,i+m+1,i+m)} - P_{(i,i-1,i+1,i+2,\dots,i+m)})R^{(i,i+m)}(k). \quad (\text{S20})$$

The part related to the inverse cycle of Eq. (S13) can be derived following the same steps. Finally, the result of the commutator, including cycle and inverse cycle (see Eq. (S4)), gives

$$\begin{aligned} [\hat{H}_{SU}, \hat{\Gamma}_{\text{red}}^{(m+1)}] &= \sum_{i=1}^{N-m-1} (P_{i\rightarrow i+m+1} + P_{i+m\rightarrow i+1} - P_{i+m+1\rightarrow i} - P_{i+1\rightarrow i+m}) (R^{(i+1,i+1+m)}(k) - R^{(i,i+m)}(k)) \\ &+ (P_{N-m+1\rightarrow N} - P_{N\rightarrow N-m+1})R^{(N-m,N)}(k) - (P_{1\rightarrow m} - P_{m\rightarrow 1})R^{(1,m+1)}(k) \\ &+ \sum_{i=1}^{N-m} \left(P_{(i,\dots,i+m-1,i+m+1,i+m)} - P_{(i,i-1,i+1,\dots,i+m)} + P_{(i+m,\dots,i+1,i-1,i)} \right. \\ &\left. - P_{(i+m,i+m+1,i+m-1,\dots,i)} \right) R^{(i,i+m)}(k), \end{aligned} \quad (\text{S21})$$

which is nonzero in general.

We remark that, in the case of periodic boundary condition, $R^{(i,i+m)}$ depends only on m and therefore the first-line contribution in Eq. S21 is zero. The second line is zero by shifting $N - m + 1 \rightarrow 1$ which it is possible in case of periodic boundary conditions. The last remaining contribution in Eq. (S21) can be written as

$$2 \sum_{i=1}^N \left(P_{(i,i+1,\dots,i+m-1,i+m+1,i+m)} - P_{(i,i+1,\dots,i+m-1,i+m+1,i+m)}^{-1} \right) R^{(i,i+m)}(k), \quad (\text{S22})$$

where we have used parity ($x \rightarrow N + 1 - x$) and the change of variable $j = N + 1 - m - i$ to collect the terms (Eq. (S22) is twice Eq. (S19) after this change of variable and the factor 2 takes into account the cycle and inverse cycle). Therefore, this commutator is also nonzero in case of periodic boundary conditions.

II. TAN'S RELATION IN THE SPIN DYNAMICS

In this Section, we show that the Tan relation that relates the asymptotic behavior of the momentum distribution for large k and the expectation value of the derivative of the Hamiltonian with respect to the inverse of the interaction strength still holds in the nonequilibrium scenario presented in this work. This relation derives from the ‘‘adiabatic sweep theorem’’, which was first demonstrated by Tan [5, 6] at thermal equilibrium, but it is not valid in general. Indeed, deviations from this relation have been especially found for nonequilibrium systems [7–10]. Moreover, as mentioned in the main text, we remark that the finite size of the system can also alter this relation in a box trap with rigid borders [11, 12] by adding extra terms in the k^4 tail which are dependent on the size of the system. Those additional terms, called \mathcal{C}_b in the the main text, do depend on L and N and eventually oscillate in momentum space, but do not contribute to the symmetry oscillations studied in this work and therefore we will neglect them in this section. A study of these oscillations for the spin-mixing dynamics will be the subject of an upcoming publication.

Our goal is to demonstrate that, in the large k limit and in the presence of smooth confinement, the total momentum distribution multiplied by k^4 behaves as

$$\lim_{k\rightarrow\infty} k^4 n(k, t) = \mathcal{C}_T(t) = -\frac{m^2}{\pi\hbar^4} \left(\langle \Psi(t) | \frac{\partial \hat{H}}{\partial 1/g_{\uparrow\downarrow}} | \Psi(t) \rangle + \sum_{\sigma=\uparrow,\downarrow} \langle \Psi(t) | \frac{\partial \hat{H}}{\partial 1/g_{\sigma\sigma}} | \Psi(t) \rangle \right), \quad (\text{S23})$$

where $|\Psi(t)\rangle$ is the many-body wave function (Eq.(2) of the main text in Dirac notation).

First, we look at the left side of Eq. (S23) and we re-write the momentum distribution as

$$\begin{aligned} n(k, t) &= \sum_{i,j=1}^N c^{(i,j)}(t) R^{(i,j)}(k) \\ &= \frac{N!}{2\pi} \sum_{i,j} c^{(i,j)}(t) \int_{I_{ij}} \left(\prod_{n \neq i}^N dx_n \right) \left| \int dx e^{-ikx} \Psi_A(x_1 \cdots, x_{i-1}, x, x_{i+1}, \cdots x_N) \right|^2, \end{aligned} \quad (\text{S24})$$

where $I_{ij} = \{x_1 < \cdots < x_{i-1} < x < x_{i+1} < \cdots < x_j < x' < x_{j+1} < \cdots < x_N\}$ is the integration range defined in the main text and the spin coefficients $c^{(i,j)}(t)$ are given by

$$c^{(i,j)}(t) = \langle \chi(t) | \hat{P}_{(i,\dots,j)} | \chi(t) \rangle. \quad (\text{S25})$$

In the large- k limit, the Fourier transform is dominated by the contribution of the short-distance divergence coming from the contact condition [13–15]. In this limit, the strongly-interacting many-body wave function can be written in the form

$$\Psi_A(\vec{X}) \stackrel{|x_i - x_j| \rightarrow 0}{\approx} |x_i - x_j| \mathcal{A} \left(\frac{x_i + x_j}{2}, x_{n \neq i,j} \right), \quad (\text{S26})$$

where $|x_i - x_j|$ is the two-body wave function satisfying the two-body Schrödinger equation in the Tonks limit and \mathcal{A} is a regular function of the center of mass of x_i and x_j and the rest of the coordinates. Importantly, we notice that here we use the Tonks-Girardeau basis instead of the Slater determinant to include the singular behavior at short distances directly in Ψ_A . One can then use Eq. (S26) to evaluate the Fourier transform in Eq. (S24):

$$\begin{aligned} & \int dx e^{-ikx} \Psi_A(x_1 \cdots x \cdots x_N) \stackrel{|x - x_l| \rightarrow 0}{\approx} \int dx \sum_{l \neq i} e^{-ikx} \mathcal{A}(x, x_{n \neq i,l}) |x - x_l| \\ &= -\frac{2}{k^2} \sum_{l \neq i}^N \mathcal{A}(x, x_{n \neq i,l}) e^{-ikx_l}, \end{aligned} \quad (\text{S27})$$

where we have used that $\lim_{k \rightarrow \infty} \int dx e^{-ikx} f(x) = 2 \cos(\pi(\alpha + 1)/2) \Gamma(\alpha + 1) \exp(-ikx_0) F(x_0) / |k|^{\alpha+1} + o(1/|k|^{\alpha+2})$ if $f(x)$ has a singularity of the type $|x - x_0|^\alpha F(x)$ at x_0 and $F(x)$ is analytic and $\alpha > -1, \alpha \neq 0, 2, 4, \dots$ [13, 16]. Notice that the assumption that at large k only short-distance correlations count is not always guaranteed out-of-equilibrium, where the correlations can spread in time, see Ref. [7] for deep quenches.

By inserting Eq. (S27) into Eq. (S24), we find that

$$\begin{aligned} \lim_{k \rightarrow \infty} k^4 n(k, t) &= \frac{N!}{2\pi} \sum_{i,j} c^{(i,j)}(t) \int_{I_{ij}} \left(\prod_{n \neq i}^N dx_n \right) \frac{4}{k^4} \sum_{l \neq i} \sum_{m \neq i} \mathcal{A}^*(x, x_{n \neq i,l}) \mathcal{A}(x', x_{n \neq i,m}) e^{-ik(x_m - x_l)} \\ & \stackrel{|x - x'| \rightarrow 0}{\approx} \frac{2N!}{\pi} \sum_{i=1}^{N-1} \left(c^{(i,i+1)}(t) + c^{(i,i)}(t) \right) \sum_{l \neq i} \int_{K_i} \left(\prod_{n \neq i}^N dx_n \right) |\mathcal{A}(x, x_{n \neq i,l})|^2, \end{aligned} \quad (\text{S28})$$

where the off diagonal terms ($l \neq m$), which are multiplied by a product of regular functions, $\mathcal{A}^* \mathcal{A}$, are neglected because they vanish faster than $1/k^4$ due to Riemann – Lebesgue lemma [16], $K_i = \{x_1 < \cdots < x_{i-1} < x \leq x' < x_{i+1} < \cdots < x_N\}$ such that the only j that survives in the sum are $j = i$ ($x = x'$) and $j = i + 1$ ($x \lesssim x'$). Therefore, as mentioned in the main text, Eq. (S28) only depends on short distance correlations, which means that, at large k , only the terms with $m = 0$ and 1 contributes in Eq. (S4) and $R^{(i,i+m)}(k)$ does not depends on i , and therefore \hat{n}_k depends only on $\hat{\Gamma}_{\text{red}}^{(1)} + \hat{\Gamma}_{\text{red}}^{(2)}$, whose second term is proportional to the Hamiltonian itself (and therefore, they can commute).

We now demonstrate the right side of Eq. (S23), namely Eq. (S28) is equal to the Tan contact. To do so, we consider the spin Hamiltonian in Eq. (3) of the main text, where the spatial part of the wave function is already integrated

out. Therefore, one can write the right side of Eq. (S23) as

$$\begin{aligned}
-\frac{m^2}{\pi\hbar^4} \left(\langle \chi(t) | \frac{\partial \hat{H}_s}{\partial 1/g_{\uparrow\downarrow}} | \chi(t) \rangle + \sum_{\sigma=\uparrow,\downarrow} \langle \chi(t) | \frac{\partial \hat{H}_s}{\partial 1/g_{\sigma\sigma}} | \chi(t) \rangle \right) &= \frac{m^2}{\pi\hbar^4} \sum_{i=1}^{N-1} 2\alpha_i \langle \chi(t) | \left(\vec{S}_i \vec{S}_{i+1} + \frac{3}{4} \right) | \chi(t) \rangle \\
&= \frac{m^2}{\pi\hbar^4} \sum_{i=1}^{N-1} \alpha_i \langle \chi(t) | (P_{i,i+1} + 1) | \chi(t) \rangle \\
&= \frac{m^2}{\pi\hbar^4} \sum_{i=1}^{N-1} \alpha_i \left(c^{(i,i+1)}(t) + c^{(i,i)}(t) \right),
\end{aligned} \tag{S29}$$

where, in the second line, we have used that the definition of the swapping operator in terms of spin operators, namely $P_{i,i+1} = 2\vec{S}_i \vec{S}_{i+1} + 1/2$ [4] and, in the third line, we have introduced the spin coefficients (see Eq. (S25)). By recalling the derivation of Ref. [17], the spatial part, α_i (Eq. (4) of the main text), can be re-written as

$$\begin{aligned}
\alpha_i &= \lim_{g_{\sigma\sigma'} \rightarrow \infty} g_{\sigma\sigma'}^2 \frac{N!}{2} \sum_{l \neq i} \int d\vec{X} \delta(x_i - x_l) \theta_{\text{Id}}(\vec{X}) \theta_P(\vec{X}) \Psi_A^*(\vec{X}) \Psi_A^*(\vec{X}) \\
&= \lim_{g_{\sigma\sigma'} \rightarrow \infty} g_{\sigma\sigma'}^2 \frac{N!}{2} \sum_{l \neq i} \int_{K_i} \prod_{n \neq i} dx_n \Psi_A^*(x_1, \dots, x_i = x_l, \dots, x_i = x_l, \dots, x_N) \Psi_A(x_1, \dots, x_i = x_l, \dots, x_i = x_l, \dots, x_N),
\end{aligned} \tag{S30}$$

where K_i is the same integration interval of Eq. (S28) except for $x \rightarrow x_i$ and $x' \rightarrow x_j$. Then, if one considers the cusp condition [18], namely

$$\frac{mg_{\sigma\sigma'}}{\hbar^2} \Psi_A |_{x_i=x_l} = \frac{\partial \Psi_A}{\partial (x_i - x_l)} \Big|_{0-}^{0+} \Big|_{|x_i-x_l| \rightarrow 0} \approx 2\mathcal{A}(x_i, x_{n \neq i, l}), \tag{S31}$$

where the function \mathcal{A} derives from the short-range expansion in Eq. (S26), Eq. (S30) becomes

$$\alpha_i = \frac{2N!\hbar^4}{m^2} \sum_{l \neq i} \int_{K_i} \prod_{n \neq i} dx_n \left| \mathcal{A}(x_i, x_{n \neq i, l}) \right|^2. \tag{S32}$$

Finally, by inserting Eq. (S32) in Eq. (S29), we find

$$\mathcal{C}_T(t) = \frac{2N!}{\pi} \sum_{i=1}^{N-1} \left(c^{(i,i+1)}(t) + c^{(i,i)}(t) \right) \sum_{l \neq i} \int_{K_i} \prod_{n \neq i} dx_n \left| \mathcal{A}(x_i, x_{n \neq i, l}) \right|^2, \tag{S33}$$

which is equivalent to Eq. (S28).

III. ANALYTICAL EXPRESSIONS FOR $N = 4$

In Fig.(3) of the main text we compare the symmetry oscillations of the expectation value of $\Gamma^{(2)}$ with the one of the momentum distribution at fixed k for $N = 6$ in a box potential. The two observables do not oscillate exactly with the same frequencies due to the fact that the eigenvalues of $\Gamma^{(2)}$, γ_ℓ , are degenerate contrary to the eigenvalues of \hat{n}_k , $n_\ell(k)$. For the sake of illustration, we provide here the analytical expressions for $\gamma_2(t)$ and \mathcal{C}_T for the symmetry-breaking case of 4 particles.

Initially, we write $\hat{\Gamma}^{(2)}$ (Eq.(7) of the main text) and \hat{H}_{SU} (Eq. (S9)) in the following basis $\{|\uparrow\uparrow\downarrow\downarrow\rangle, |\uparrow\downarrow\uparrow\downarrow\rangle, |\downarrow\uparrow\uparrow\downarrow\rangle, |\uparrow\downarrow\downarrow\uparrow\rangle, |\downarrow\uparrow\downarrow\uparrow\rangle, |\downarrow\downarrow\uparrow\uparrow\rangle\}$, the so-called ‘‘snippet’’ basis [18], as following

$$\hat{\Gamma}^{(2)} = \begin{pmatrix} 2 & 1 & 1 & 1 & 1 & 0 \\ 1 & 2 & 1 & 1 & 0 & 1 \\ 1 & 1 & 2 & 0 & 1 & 1 \\ 1 & 1 & 0 & 2 & 1 & 1 \\ 1 & 0 & 1 & 1 & 2 & 1 \\ 0 & 1 & 1 & 1 & 1 & 2 \end{pmatrix}, \quad \hat{H}_{SU} = \begin{pmatrix} 5 & 1 & 0 & 0 & 0 & 0 \\ 1 & 3 & 1 & 1 & 0 & 0 \\ 0 & 1 & 4 & 0 & 1 & 0 \\ 0 & 1 & 0 & 4 & 1 & 0 \\ 0 & 0 & 1 & 1 & 3 & 1 \\ 0 & 0 & 0 & 0 & 1 & 5 \end{pmatrix}. \tag{S34}$$

The matrices in Eq. (S34) are simultaneously diagonalized using the basis

$$|\gamma_0\rangle = a_0 \begin{pmatrix} 1 \\ 1 \\ 1 \\ 1 \\ 1 \end{pmatrix}, \quad |\gamma_1\rangle = \begin{pmatrix} -a_1 \\ -a_2 \\ 0 \\ 0 \\ a_2 \\ a_1 \end{pmatrix}, \quad |\gamma_2\rangle = \begin{pmatrix} -a_3 \\ a_4 \\ a_0 \\ a_0 \\ a_4 \\ -a_3 \end{pmatrix}, \quad |\gamma_3\rangle = a_5 \begin{pmatrix} 0 \\ 0 \\ 1 \\ -1 \\ 0 \\ 0 \end{pmatrix}, \quad |\gamma_4\rangle = \begin{pmatrix} a_2 \\ -a_1 \\ 0 \\ 0 \\ a_1 \\ -a_2 \end{pmatrix}, \quad |\gamma_5\rangle = \begin{pmatrix} a_4 \\ -a_3 \\ a_0 \\ a_0 \\ -a_3 \\ a_4 \end{pmatrix}, \quad (\text{S35})$$

with $a_0 = 1/\sqrt{6}$, $a_1 = 0.6532$, $a_2 = 0.2706$, $a_3 = 0.5577$, $a_4 = 0.1494$, $a_5 = 1/\sqrt{2}$. The eigenvectors in Eq. (S35) are ordered in decreasing \hat{H}_{SU} -eigenvalues, namely $\epsilon_\ell^{\text{SU}} = \{6(\gamma_0 = 6), 5.41(\gamma_1 = 2), 4.73(\gamma_2 = 0), 4(\gamma_3 = 2), 2.58(\gamma_4 = 2), 1.26(\gamma_5 = 0)\}$ in units of the coupling coefficient α (Eq.(4) of the main text) and where γ_ℓ in parenthesis are the corresponding $\hat{\Gamma}^{(2)}$ -eigenvalues.

We then decompose the spin state in the energy basis, namely $|\chi(t)\rangle = \sum_n s_n e^{-iE_n t} |\chi_n\rangle$ with s_n real coefficients and $|\chi_n\rangle$ eigenvectors of \hat{H}_{SB} , which reads, in the snippet basis, as

$$\hat{H}_{\text{SB}} = \begin{pmatrix} 1 & 1 & 0 & 0 & 0 & 0 \\ 1 & 3 & 1 & 1 & 0 & 0 \\ 0 & 1 & 2 & 0 & 1 & 0 \\ 0 & 1 & 0 & 2 & 1 & 0 \\ 0 & 0 & 1 & 1 & 3 & 1 \\ 0 & 0 & 0 & 0 & 1 & 1 \end{pmatrix}. \quad (\text{S36})$$

The eigenvectors $|\chi_n\rangle$ can be expressed in terms of the basis in Eq. (S35) as follows

$$\begin{aligned} |\chi_0\rangle &= -0.911 |\gamma_0\rangle - \frac{1}{3} |\gamma_2\rangle + 0.244 |\gamma_5\rangle \\ |\chi_1\rangle &= -\frac{1}{\sqrt{2}} (|\gamma_1\rangle + |\gamma_4\rangle) \\ |\chi_2\rangle &= -|\gamma_3\rangle \\ |\chi_3\rangle &= -0.244 |\gamma_0\rangle + 0.911 |\gamma_2\rangle + \frac{1}{3} |\gamma_5\rangle \\ |\chi_4\rangle &= \frac{1}{\sqrt{2}} (-|\gamma_1\rangle + |\gamma_4\rangle) \\ |\chi_5\rangle &= \frac{1}{3} |\gamma_0\rangle - 0.244 |\gamma_2\rangle + 0.911 |\gamma_5\rangle \end{aligned} \quad (\text{S37})$$

By projecting into the $\{|\gamma_\ell\rangle\}$ basis, the evolution of the expectation value of $\hat{\Gamma}^{(2)}$ can be written as

$$\begin{aligned} \gamma^{(2)}(t) &= \sum_{m,n=0}^5 s_n s_m \sum_{\ell=0}^5 \langle \chi_n | \gamma_\ell \rangle \gamma_\ell \langle \gamma_\ell | \chi_m \rangle e^{-i(E_n - E_m)t} \\ &= 6(0.83s_0^2 + 0.06s_3^2 + 0.11s_5^2) + 2(s_1^2 + s_2^2 + s_4^2) \\ &\quad + 2.62s_0s_3 \cos((E_3 - E_0)t) - 3.60s_0s_5 \cos((E_5 - E_0)t) - 0.95s_3s_5 \cos((E_5 - E_3)t), \end{aligned} \quad (\text{S38})$$

which oscillates in time with three different frequencies $\omega_{30} = E_3 - E_0$, $\omega_{50} = E_5 - E_0$, and $\omega_{35} = E_3 - E_5$.

We then repeat the same steps for the Tan contact (Eq. (S23)), and we obtain

$$\begin{aligned} \mathcal{C}_T(t) &= \sum_{m,n=0}^5 s_n s_m \sum_{\ell=0}^5 \langle \chi_n | \gamma_\ell \rangle \lambda_\ell \langle \gamma_\ell | \chi_m \rangle e^{-i(E_n - E_m)t} \\ &= s_0^2(0.91^2\lambda_0 + 0.33^2\lambda_2 + 0.24^2\lambda_5) + s_3^2(0.24^2\lambda_0 + 0.91^2\lambda_2 + 0.33^2\lambda_5) \\ &\quad + s_5^2(0.33^2\lambda_0 + 0.24^2\lambda_2 + 0.91^2\lambda_5) + (s_1^2 + s_4^2)(0.707^2\lambda_1 + 0.707^2\lambda_4) + s_2^2\lambda_3 \\ &\quad + s_0s_3 \cos((E_3 - E_0)t)[0.22\lambda_0 - 0.3\lambda_2 + 0.08\lambda_5] + s_0s_5 \cos((E_5 - E_0)t)[-0.3\lambda_0 + 0.07\lambda_2 + 0.22\lambda_5] \\ &\quad + s_3s_5 \cos((E_5 - E_3)t)[-0.07\lambda_0 - 0.22\lambda_2 + 0.3\lambda_5] + s_1s_4 \cos((E_4 - E_1)t)[0.707\lambda_1 - 0.707\lambda_4], \end{aligned} \quad (\text{S39})$$

where $\lambda_\ell = \lim_{k \rightarrow \infty} k^4 n_\ell(k) = -m^2/(\pi \hbar^4) \langle \gamma_\ell | \left(\partial \hat{H}_{\text{SB}} / \partial g_{\uparrow\downarrow} \right) | \gamma_\ell \rangle$. Eq. (S39) oscillates with four different frequencies $\omega_{30} = E_3 - E_0$, $\omega_{50} = E_5 - E_0$, $\omega_{35} = E_3 - E_5$, and $\omega_{14} = E_4 - E_1$. In conclusion, $\mathcal{C}_T(t)$ oscillates with an additional

frequency (ω_{14}) with respect to $\gamma^{(2)}(t)$ and this originates from the fact that $\lambda_1 \neq \lambda_4$ (non-degenerate eigenvalues), but $\gamma_1 = \gamma_4 = 2$.

-
- [1] F. Deuretzbacher, D. Becker, and L. Santos, Phys. Rev. A **94**, 023606 (2016).
 - [2] A. Auerbach, *Interacting Electrons and Quantum Magnetism*, Graduate Texts in Contemporary Physics (Springer New York, 2012).
 - [3] D. P. Arovas and A. Auerbach, Phys. Rev. B **38**, 316 (1988).
 - [4] G.-M. Zhang and X. Wang, Journal of Physics A: Mathematical and General **39**, 8515–8526 (2006).
 - [5] S. Tan, Ann. Phys. **323**, 2952 (2008).
 - [6] S. Tan, Ann. Phys. **323**, 2971 (2008).
 - [7] J. P. Corson and J. L. Bohn, Phys. Rev. A **94**, 023604 (2016).
 - [8] V. E. Colussi, H. Kurkjian, M. Van Regemortel, S. Musolino, J. van de Kraats, M. Wouters, and S. J. J. M. F. Kokkelmans, Phys. Rev. A **102**, 063314 (2020).
 - [9] I. Bouchoule and J. Dubail, Phys. Rev. Lett. **126**, 160603 (2021).
 - [10] C. Rylands, P. Calabrese, and B. Bertini, Phys. Rev. Lett. **130**, 023001 (2023).
 - [11] G. Aupetit-Diallo, S. Musolino, M. Albert, and P. Vignolo, Phys. Rev. A **107**, L061301 (2023).
 - [12] B. De Bruyne, D. S. Dean, P. Le Doussal, S. N. Majumdar, and G. Schehr, Phys. Rev. A **104**, 013314 (2021).
 - [13] M. Olshanii and V. Dunjko, Phys. Rev. Lett. **91**, 090401 (2003).
 - [14] F. Werner and Y. Castin, Phys. Rev. A **86**, 013626 (2012).
 - [15] F. Werner and Y. Castin, Phys. Rev. A **86**, 053633 (2012).
 - [16] O. I. Pătu and A. Klümper, Phys. Rev. A **96**, 063612 (2017).
 - [17] F. Deuretzbacher, D. Becker, J. Bjerlin, S. M. Reimann, and L. Santos, Phys. Rev. A **90**, 013611 (2014).
 - [18] A. Minguzzi and P. Vignolo, AVS Quantum Science **4**, 027102 (2022).